

# Outstanding performance of hierarchical alumina microspheres for boron removal in the presence of competing ions

Xiang-Yang Lou<sup>a,\*</sup>, Roberto Boada<sup>a,\*</sup>, Lucia Yohai<sup>a,b</sup>, Manuel Valiente<sup>a</sup>

<sup>a</sup> GTS-UAB Research Group, Department of Chemistry, Facultat de Ciències, Universitat Autònoma de Barcelona, 08193 Bellaterra, Spain

<sup>b</sup> Instituto de Investigaciones en Ciencia y Tecnología de Materiales (INTEMA, UNMdP-CONICET), B7608FDQ Mar del Plata, Argentina

## ARTICLE INFO

### Keywords:

Boron  
Adsorption  
Gamma-phase hierarchical alumina microspheres  
Competing ions  
Regeneration

## ABSTRACT

Developing efficient materials for the removal of boron from aqueous solutions is becoming an important task to overcome boron pollution. Herein, we present hierarchical alumina microspheres (HAM) as an outstanding adsorbent, synthesized via a microwave-assisted co-precipitation method. The microstructure, morphology, and textural characterization of the HAM particles carried out by X-ray diffraction (XRD), scanning electron microscopy (SEM), and transmission electron microscopy (TEM) revealed hollow  $\gamma$ - $\text{Al}_2\text{O}_3$  particles with a porous dandelion-like shape and an average size of 1.5  $\mu\text{m}$ . The analysis of the adsorption data indicated that the adsorption was homogeneous in a single layer and that chemical adsorption was the controlling step in the process. The adsorption capacity obtained at an initial concentration of 800  $\text{mg}\cdot\text{L}^{-1}$  was 51.60  $\text{mg}\cdot\text{g}^{-1}$ , and the theoretically calculated maximum adsorption capacity using the Langmuir model was 138.50  $\text{mg}\cdot\text{g}^{-1}$ , which outperforms previously reported adsorbents. The determination of thermodynamic parameters indicated that the adsorption is an exothermic and non-spontaneous process. The XPS spectra of HAM after adsorption indicated the formation of Al-O-B bonds. Of particular interest for industrial applications, the HAM adsorbent showed excellent selectivity for boron in the presence of competing cations or anions and at different ionic strengths. In addition, HAM maintained a high adsorption capacity after five consecutive adsorption/desorption cycles. These findings highlight the potential of HAM as a highly microporous material for boron removal in real industrial applications.

## 1. Introduction

Boron (B) is an essential micronutrient for plants and it is released into the environment from both natural processes (e.g., weathering of rocks and leaching of salt deposits) and anthropogenic activities (e.g., the production of glass, porcelain, semiconductors) [1,2]. The average boron concentration found in the environment varies strongly depending on the media: 9–85  $\text{mg}\cdot\text{kg}^{-1}$  in soil [3], 4.5  $\text{mg}\cdot\text{L}^{-1}$  in seawater [4], 0.3–100  $\text{mg}\cdot\text{L}^{-1}$  in groundwater [5], 0.01–200  $\text{mg}\cdot\text{L}^{-1}$  in surface-water [6], and higher than 100  $\text{mg}\cdot\text{L}^{-1}$  in sewage wastewater [7]. Unfortunately, the presence of high concentrations of boron causes environmental (e.g., acid rain and crop poisoning) and human health issues (e.g., kidney damage, anorexia, and diarrhea) [8]. Indeed, the World Health Organization (WHO) has established a guideline value of 2.4  $\text{mg}\cdot\text{L}^{-1}$  as the upper limit for boron in drinking water [9]. Taking into account the toxicity of concentrated boron in groundwater and surface water, and the need for removing boron from wastewater and seawater

during desalination procedures, the development of effective boron remediation processes has become an important task [10].

The presence of different chemical boron species in water and their concentration variability imposes a great challenge for achieving an efficient and selective boron removal from polluted water [11]. Compared with other remediation methodologies, adsorption is considered to be one of the most promising approaches owing to its numerous advantages such as high efficiency, easy operation, environmentally friendly, low cost, and suitability for the removal of low concentration pollutants [12]. Various traditional adsorbents, such as activated carbon [13], fly ash [14], silica [15], biomass [16], and magnetic nanobeads [17] have been used for boron removal. The main advantages of these adsorbents are their low cost and easy accessibility. However, they have low adsorption capacities ( $<20 \text{ mg}\cdot\text{g}^{-1}$ ) and bad selectivity due to the weak interactions between the adsorbate and the adsorbents [18]. Many polyhydroxy-functionalize commercial resins have been also used for B removal because they show a high boron

\* Corresponding author.

E-mail address: [roberto.boada@uab.cat](mailto:roberto.boada@uab.cat) (R. Boada).

<https://doi.org/10.1016/j.jwpe.2023.104218>

Received 5 April 2023; Received in revised form 24 August 2023; Accepted 24 August 2023

Available online 31 August 2023

2214-7144/© 2023 The Authors. Published by Elsevier Ltd. This is an open access article under the CC BY-NC-ND license (<http://creativecommons.org/licenses/by-nc-nd/4.0/>).

selectivity [13], however, their limited chemical and thermal stability, together with their low adsorption capacities (e.g., Amberlite PWA10, LSC 780, Diaion CBR05, and Purolite S108 have an adsorption capacity within 5.9–7.2 mg·g<sup>-1</sup>) prevent them to be considered as viable adsorbents for B remediation [19]. Besides, raw materials used for synthesizing these resins are expensive, and the cost of recycling those materials is also rather high which are additional drawbacks to overcome.

In this study, we propose using hierarchical gamma-phase alumina microspheres (HAM) synthesized via microwave-assisted co-precipitation method as an alternative adsorbent for achieving effective and selective boron removal from aqueous solutions in the presence of competing ions. The high density of hydroxyl groups on the surface of  $\gamma$ -Al<sub>2</sub>O<sub>3</sub> provides abundant adsorption sites for the effective removal of pollutants from water, which has been demonstrated in numerous studies [20,21]. Besides, in contrast with the commercial resins mentioned above, the low-cost and environmentally-friendly production makes HAM a more sustainable and economically viable option for large-scale water treatment applications. Furthermore, the overall micrometer-sized structure of  $\gamma$ -Al<sub>2</sub>O<sub>3</sub> particles provides several advantages over other nanoscale adsorbents. It reduces the aggregation of particles in solution, which enhances their dispersibility and prevents the formation of filter cake during the filtration process. This, in turn, results in better mechanical strength, facile transportation, and easy recovery of the adsorbent, making it a practical option for real-world water treatment applications [22,23].

## 2. Materials and methods

### 2.1. Chemical reagents

All chemicals used in the experiments were of analytical grade and purchased from Sigma-Aldrich (Missouri, USA), Panreac (Barcelona, Spain), Scharlab (Barcelona, Spain), or Honeywell, (Charlotte, USA).

Aluminum potassium sulfate dodecahydrate (KAl(SO<sub>4</sub>)<sub>2</sub>·12H<sub>2</sub>O) and urea (CO(NH<sub>2</sub>)<sub>2</sub>) were used to synthesize HAM. The source of boron was boric acid, B(OH)<sub>3</sub>. An aqueous stock solution of 1000 mg·L<sup>-1</sup> boron was first prepared and then diluted as required. Hydrochloric chloride (HCl) and sodium hydroxide (NaOH) were used to adjust the pH of the solutions in the synthesis and adsorption processes. Carmine (C<sub>22</sub>H<sub>20</sub>O<sub>13</sub>) and sulfuric acid (H<sub>2</sub>SO<sub>4</sub>) were used for the detection of boron by the carmine colorimetric method as reported elsewhere [24]. The method is described in detail in Section S1 in the Supplementary information (SI).

### 2.2. Microwave-assisted synthesis of HAM

HAM was synthesized using a microwave (MARS-5, CEM, Matthews, North Carolina, USA) assisted methodology following previously reported works [25]. In brief, a 100 ml aqueous solution of aluminum potassium sulfate dodecahydrate (0.05 M) and urea (0.10 M) was stirred at 300 rpm for 15 min. The resulting solution was divided into seven microwave vessels of 100 ml using a graduated cylinder, then heated at 180 °C for 20 min setting the microwave power to 1000 W. Once cooled down to room temperature, the pH was adjusted to ~9.0 by adding 1 M NaOH solution (the initial pH of the solution was ~7.2). The resulting solid material was collected by centrifugation (3000 rpm, 5 min) and washed with hot Milli-Q water (70 °C) and ethanol to remove the excess chemicals. The collected precipitate was dried in an oven at 80 °C for 12 h. The dried precipitate was calcinated in a muffle at 600 °C for 2 h. After cooling down to room temperature, the lump of material finally obtained was broken down by gently grinding and stored for future use. A diagram of the HAM synthesis is displayed in Fig. S1.

### 2.3. Characterizations of HAM

The morphology and size of the HAM particles were studied by

scanning electron microscope, SEM (Merlin, Carl Zeiss AG, Oberkochen, Germany) and transmission Electron Microscope, TEM (JEM-1400, JEOL, Tokyo, Japan). The SEM images were analyzed using Image-pro Plus software to determine the particle size distribution. X-ray powder diffraction, XRD (X-Pert, Philips, Amsterdam, Netherlands) was carried out to identify the crystallographic phase of HAM. Fourier-transform infrared spectroscopy, FTIR (Nicolet iS10, Waltham, America), and X-ray photoelectron spectroscopy, XPS (Thermo Scientific K-Alpha, Waltham, America) analysis were performed to study the adsorption mechanism.

The point of zero charge (pH<sub>pzc</sub>) of HAM was detected using the pH drift method [26]. Various flasks were filled with 30 ml of 0.01 M KNO<sub>3</sub> solutions. The pH of these solutions was adjusted to get a pH from 2.0 to 10.0 using 0.1 M HCl and NaOH solutions. Subsequently, 0.1 g of adsorbent was added to each solution, and the pH was measured again after 48 h. The pH<sub>pzc</sub> is determined as the pH value at which the initial and final pH values are identical.

### 2.4. Adsorption and desorption experiments

Boron adsorption experiments were performed in 50 ml plastic tubes containing 25 ml of boron solution and 0.1 g of adsorbent. The tubes were agitated mechanically at 300 rpm, and the experiments were performed at different temperatures: 293, 318, and 343 K. The solutions were separated from the adsorbents by centrifugation (3000 rpm, 5 min), and the concentration of the unadsorbed boron was determined by the carmine colorimetric UV-Vis method (see Section S2 for further details). The adsorption capacity at equilibrium ( $q_e$ ) was calculated using the following equation:

$$q_e = (C_o - C_e) \frac{V}{m} \quad (1)$$

where  $q_e$  (mg·g<sup>-1</sup>) is the adsorption capacity,  $V$  (L) is the volume of the solution,  $m$  (g) is the weight of the adsorbent,  $C_o$  and  $C_e$  (mg·L<sup>-1</sup>) are initial and equilibrium concentrations of boron, respectively.

Desorption experiments were performed using 25 ml of 0.1 M HCl solution and agitating for 2 h. The adsorbents were separated by centrifugation and the adsorption/desorption cycle was repeated several times to assess the regeneration capabilities.

### 2.5. Effect of competing ions and different ion strength

To examine the competing effects in the boron adsorption procedure due to the presence of other ions that may be present in natural systems, a 1:1 molar concentration mixture of each ion (cations or anions) and boron was used with an initial concentration of 18.50 mM (200 mg·L<sup>-1</sup> for boron). This concentration was chosen considering the boron concentration in real wastewater of oil/gas excavation, geothermal water, mining, metal-processing, or semiconductor industries as reported by Lin et al. [6]. Besides, to account for the composition of wastewater in real conditions, experiments with a higher concentration ratio of different anions ([B]:[anion], 1:100), were also performed. Different salt reagents were used as cation sources (NaCl, KCl, CaCl<sub>2</sub>, MgCl<sub>2</sub>), metal sources (Ni(NO<sub>3</sub>)<sub>2</sub>·4H<sub>2</sub>O, Cu(NO<sub>3</sub>)<sub>2</sub>·6H<sub>2</sub>O, Cr(NO<sub>3</sub>)<sub>2</sub>·6H<sub>2</sub>O and Fe(NO<sub>3</sub>)<sub>2</sub>·6H<sub>2</sub>O) and anion sources (NaCl, NaNO<sub>3</sub>, Na<sub>2</sub>SO<sub>4</sub>·10H<sub>2</sub>O, Na<sub>3</sub>PO<sub>4</sub>·12H<sub>2</sub>O). The adsorption experiments were performed at pH 8.0. To examine the effect of the ion strength of the solution on the boron adsorption capacity, a series of adsorption experiments were performed by adding NaCl to the boron solution within the range 0–58.44 g·L<sup>-1</sup>. To further examine the competitive adsorption of boron under real conditions, simulated tap water and ground water polluted with boron were prepared. The compositions of these samples are provided in Section S3 and Table S1.

### 3. Results and discussion

#### 3.1. Characterization of HAM

The morphology study of HAM provided information about the shape, average size, and size distribution of the synthesized particles. SEM images (Fig. 1a) showed that HAM are hollow particles with a highly textured surface and porous dandelion shape. This structure provides a large specific surface area (ca.  $250 \text{ m}^2\text{g}^{-1}$ ) [25], which would benefit the boron adsorption. The average size of HAM particles was  $1.5 \pm 0.5 \mu\text{m}$ . These values are similar to those reported in previous works following a similar synthesis procedure [25]. The hollow and porous dandelion morphology of the HAM particle was confirmed in the TEM image (Fig. 1b). Besides, the size of HAM determined from TEM images was consistent with the results from SEM characterization. In addition, XRD was used to identify the crystal structure of the synthesized HAM particles. The diffraction pattern obtained, Fig. 1c, corresponds to the structure reported for  $\gamma\text{-Al}_2\text{O}_3$  (Crystallography Open Database ID: 2015530) [27]. Even though the diffraction peaks of the HAM particles are rather wide due to the nanosized wall thickness of the hierarchical structure, the main reflections are matching those obtained from the simulation of the  $\gamma\text{-Al}_2\text{O}_3$  structure.

#### 3.2. Effect of pH

In water, boron speciation is influenced by the pH and the concentration of the solution (see Fig. S2). The most common species of boron are boric acid,  $\text{B}(\text{OH})_3$ , and various kinds of borates (e.g.,  $\text{B}(\text{OH})_4^-$ ) [28]. Boric acid and borate oxyanion,  $\text{B}(\text{OH})_4^-$ , are mainly present at low concentrations ( $<216.2 \text{ mg}\cdot\text{L}^{-1}$ ). Boric acid dominates at low pH values, while borate ions dominate at high pH values. At high concentrations ( $>270.3 \text{ mg}\cdot\text{L}^{-1}$ ), water-soluble polyborate ions such as  $\text{B}_2(\text{OH})_5^-$ ,  $\text{B}_3\text{O}_3(\text{OH})_4^-$ , and  $\text{B}_4\text{O}_5(\text{OH})_4^{2-}$  are formed with an increase of pH value from 6.0 to 10.0 [29]. Therefore, pH is an important parameter that should be investigated when studying boron adsorption [30]. The boron adsorption capacity of HAM with  $200 \text{ mg}\cdot\text{L}^{-1}$  initial concentration,  $0.1 \text{ g}$  of the adsorbent per  $25 \text{ ml}$  solution,  $120 \text{ min}$  contact times at  $293 \text{ K}$  as a function of pH is shown in Fig. 2a.

The results show that within the pH range studied, the adsorption capacity increases with the pH until reaching a plateau around 6.0–7.0 which is followed with a further increase reaching a maximum ( $14.92 \text{ mg}\cdot\text{g}^{-1}$ ) at around 8.0. For higher pH, a slight decrease is found. These results are related to the change in the fraction of the boron species present as a function of pH and influenced by the charge of the HAM surface that varies as a function of the pH. As reported, alumina has considerably strong Lewis acidity and little Brönsted acidity [22]. The  $\text{pH}_{\text{PZC}}$  of HAM was determined by the pH drift method. Fig. S3 shows that the  $\text{pH}_{\text{PZC}}$  of HAM is 5.9. Therefore, at pH values below 5.9, the surface of HAM is positively charged, whereas at pH values above 5.9, the surface is negatively charged.

Regarding boron, at pH values below 7.0, it exists predominant as  $\text{B}(\text{OH})_3$ , which exhibits low affinity to HAM due to the weak Lewis acid nature of boric acid. As the pH increased to 9.0,  $\text{B}(\text{OH})_3$  is converted into  $\text{B}(\text{OH})_4^-$  rapidly. These borate anions can interact favorably with amino and hydroxyl groups [31]. Despite the electrostatic repulsion between the negative surfaces of both HAM and  $\text{B}(\text{OH})_4^-$ , the dominant ion exchange of boron anions with hydroxyl groups on HAM surface led to a higher adsorption capacity of boron. At pH values above 9.0, the chemical form of boron was  $\text{B}(\text{OH})_4^-$ , and the strong electrostatic repulsion between HAM and  $\text{B}(\text{OH})_4^-$  prevailed, leading to a decrease in the adsorption capacity [32].

#### 3.3. Effect of contact time

The adsorption kinetic parameters are important to determine the efficiency and the mechanism responsible for the adsorption process [33]. In this study, different contact time experiments from 1 min to 24 h with  $200 \text{ mg}\cdot\text{L}^{-1}$  initial concentration,  $293 \text{ K}$  reaction temperature and pH 8.0 were performed. The results displayed in Fig. 2b revealed an initial sharp increase in the adsorption capacity, which might be attributed to a large number of adsorption sites initially available on the surface of HAM. After 120 min, the adsorption capacity becomes almost constant, which means that the adsorption equilibrium has been reached.

To better study the rate and mechanism of boron adsorption onto the HAM surface, the experimental kinetic data were fitted to the pseudo-first order kinetic model and pseudo-second order kinetic model. The equations of those two models are displayed in Section S6. The modeling results are shown in Fig. 2c and the parameters obtained from simulated curves are shown in Table 1. Despite obtaining a relatively good agreement with the two models ( $R^2 > 0.90$ ), the pseudo-second order kinetic model provided a better agreement. This implies that chemisorption is controlling the velocity of the adsorption process. Hence, the adsorption of boron on HAM involves valence forces and ion exchange mechanisms through the sharing/exchange of electrons between the hydroxyl groups on the adsorbent surface and boron [34,35].

#### 3.4. Effect of different initial concentrations

In our work, adsorption experiments at different initial boron concentrations from 1 to  $1000 \text{ mg}\cdot\text{L}^{-1}$ ,  $120 \text{ min}$  contact times at  $293 \text{ K}$  and pH 8.0 were performed. As can be seen in Fig. 2d, the adsorption capacity increases monotonically with the initial concentration of boron without reaching saturation within the concentration range studied. It is worth mentioning that the top-end of the concentration range is much higher than the concentration found in polluted waters targeted by this study,  $\sim 200 \text{ mg}\cdot\text{L}^{-1}$  [6].

The adsorption isotherm modeling results are displayed in Table 2. Among the three models considered (Langmuir, Freundlich, and Temkin; see Section S7), Langmuir and Freundlich models provided a good

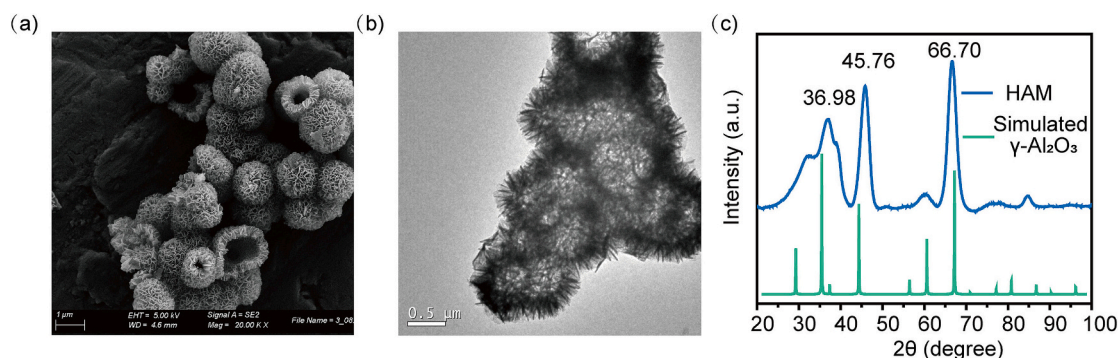
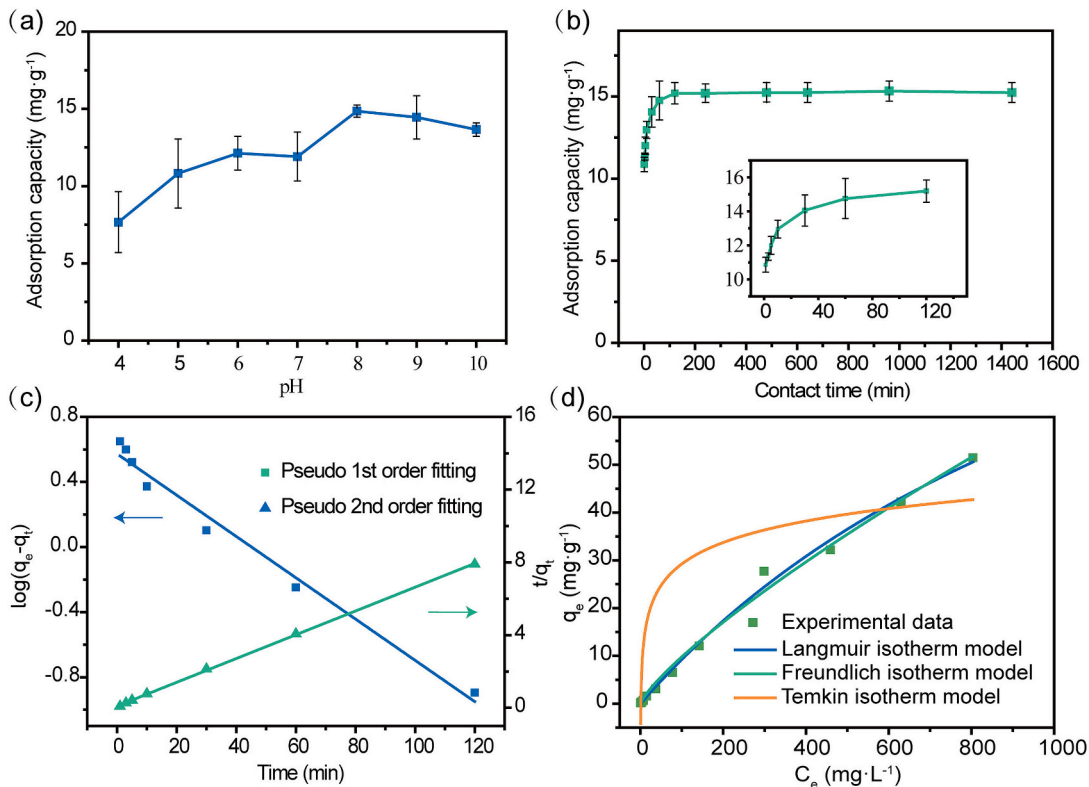


Fig. 1. Morphological and structural characterizations of synthesized HAM: SEM images (a), TEM images (b), and XRD pattern (c).



**Fig. 2.** Effect of different parameters on boron adsorption capacity of HAM: pH values (a), contact time (b), kinetic fitting (c), initial concentration with corresponding isotherm modeling (d).

**Table 1**  
Kinetic parameters obtained from the model fitting of boron adsorption on HAM: K<sub>1</sub> (min<sup>-1</sup>), K<sub>2</sub> (g·mg<sup>-1</sup>·min<sup>-1</sup>).

Kinetic model	R <sup>2</sup>	Rate constant
Pseudo-first order	0.9795	K <sub>1</sub> = 0.0290
Pseudo-second order	0.9996	K <sub>2</sub> = 0.0445

agreement ( $R^2 > 0.99$ ), however Langmuir model was the best one. This suggests that chemisorption is the main process [36–38]. Besides, for the Temkin model, the value of the regression coefficient is much worse,  $R^2 = 0.6993$ , which means that the boron adsorption process by HAM cannot be explained by this model. This points out that, in our case, the heat of adsorption does not decrease linearly with the decrease of surface coverage. The obtained adsorption capacity at 800 mg·L<sup>-1</sup> initial concentration was 51.60 mg·g<sup>-1</sup> and the theoretical maximum capacity calculated by the Langmuir model was 138.50 mg·g<sup>-1</sup> which is an outstanding value when compared with other reported materials as it will be shown below.

3.5. Thermodynamic analysis

Thermodynamic parameters such as Gibbs free energy change ( $\Delta G^\circ$ ), enthalpy change ( $\Delta H^\circ$ ), and entropy change ( $\Delta S^\circ$ ) can predict the feasibility and nature of the adsorption process.  $\Delta S^\circ$  and  $\Delta H^\circ$  were

**Table 2**  
Parameters of different isotherms models of boron adsorption by HAM. The parameters are expressed in the following units: q<sub>m</sub> (mg·g<sup>-1</sup>), K<sub>L</sub> (L·mg<sup>-1</sup>), K<sub>F</sub> [(mg·g<sup>-1</sup>)(L·mg<sup>-1</sup>)<sup>1/n</sup>], A<sub>T</sub> (L·g<sup>-1</sup>), b<sub>T</sub> (K·Jmol<sup>-1</sup>).

Langmuir isotherm			Freundlich isotherm			Temkin isotherm		
q <sub>m</sub>	K <sub>L</sub>	R <sup>2</sup>	K <sub>F</sub>	1/n	R <sup>2</sup>	A <sub>T</sub>	b <sub>T</sub>	R <sup>2</sup>
138.50	0.0007	0.9949	0.25	0.80	0.9931	0.26	0.38	0.6993

obtained from the linear fit of the Arrhenius plot (see Fig. S4, Table 3). See Section S8 for further details. Our results show that  $\Delta H^\circ$  is negative, which indicates the adsorption of boron by HAM is an exothermic process and prefers to happen at lower temperatures. However, for 293, 318, and 343 K,  $\Delta G^\circ$  was determined to be 5.18, 8.15, and 11.11 kJ·mol<sup>-1</sup>, respectively. The positive values of  $\Delta G^\circ$  for all investigated temperatures show the non-spontaneity of boron adsorption using HAM. Besides, the value of  $\Delta G^\circ$  increases by increasing the temperature which itself shows that higher temperatures result in a decreasing in the boron adsorption capacity. In addition, a decrease in randomness at the solid-solution interface during the adsorption process was indicated by the negative value of  $\Delta S^\circ$  [39].

3.6. Effect of the competing ions

To investigate the effect of competing ions on the boron adsorption by HAM, several boron adsorption experiments were performed by

**Table 3**  
Thermodynamic parameters for boron adsorption onto the HAM.

T (K)	ln K	$\Delta G^\circ$ (kJ·mol <sup>-1</sup> )	$\Delta H^\circ$ (kJ·mol <sup>-1</sup> )	$\Delta S^\circ$ (J·mol <sup>-1</sup> ·K <sup>-1</sup> )
293	-2.19	5.18	-29.59	-118.62
318	-2.94	8.15		
343	-3.97	11.11		



adding cations ( $\text{Na}^+$ ,  $\text{Mg}^{2+}$ ,  $\text{K}^+$ ,  $\text{Ca}^{2+}$ ,  $\text{Cr}^{2+}$ ,  $\text{Fe}^{2+}$ ,  $\text{Ni}^{2+}$ , and  $\text{Cu}^{2+}$ ); or anions ( $\text{Cl}^-$ ,  $\text{NO}_3^-$ ,  $\text{SO}_4^{2-}$ ,  $\text{PO}_4^{3-}$ ). The results for cations and anions are shown in Fig. 3a and b, respectively.

The boron adsorption capacity was slightly lower in the presence of most of the cations. However, in the case of  $\text{Cu}^{2+}$ ,  $\text{Cr}^{3+}$ , and  $\text{Fe}^{2+}$ , the adsorption capacity exhibited a significant increase. This notable enhancement could be attributed to the formation of hydroxide precipitates when adjusting the pH of the solution up to 8.0, as shown in Fig. S5. These hydroxide precipitates can also adsorb boron ions.

The results for the boron adsorption in the presence of the anions, Fig. 3b, show that, for the molar ratio of  $[\text{B}]:[\text{anion}] = 1:1$ , the adsorption capacity did not change noticeably and only a slight reduction is observed respect to the case without having anions, therefore these anions do not have a special affinity to HAM that could hamper the adsorption of boron. To assess the effect of the concentration of the anions, the molar ratio  $[\text{B}]:[\text{anion}]$  was increased to 1:100. In this case, boron adsorption capacities were higher than those for 1:1. For most anions, the adsorption capacity was almost identical than the case without anions. However, for  $\text{PO}_4^{3-}$ , there was a noticeable increase in the adsorption capacity. This may be related to the compression of the electrical double layer on the HAM surface due to the presence of trivalent phosphate which facilitates the interaction between the adsorption surface and the neutral boric acid species [40]. To corroborate this, boron adsorption experiments were performed at different ionic strengths by adding NaCl (0–58.44  $\text{g}\cdot\text{L}^{-1}$ , see Fig. 3c). Initially, at low ionic strength, below 2.92  $\text{g}\cdot\text{L}^{-1}$ , the adsorption capacity of boron decreased. This can be ascribed to the competing adsorption of  $\text{Na}^+$  and  $\text{Cl}^-$  ions. When the ionic strength increased from 2.92 to 58.44  $\text{g}\cdot\text{L}^{-1}$ , there is a concomitant increase in the boron adsorption. This increment can be attributed to the dominant effect of the double-layer compression over the adsorption of  $\text{Na}^+$  and  $\text{Cl}^-$  ions competing with B. In addition, this observation indicates that the mechanism of boron adsorption removal on HAM surface may be due to the formation of inner-sphere surface complexes rather than outer-sphere surface complexes. Similar

findings were also reported for boron adsorption on other metal oxide adsorbents [41,42]. The competitive adsorption of boron in simulated tap water and ground water was also investigated. As depicted in Fig. 3d, despite the presence of competitive anions and cations, the adsorption capacities of boron in tap water and ground water remained higher than 72.6 % and 80.5 %, respectively, compared to that in Milli-Q water.

### 3.7. Adsorption capacity comparison with similar adsorbent systems

As shown in Table 4, when comparing the maximum adsorption capacity of HAM with other adsorbents previously reported, we found that HAM performs better than most inorganic and organic adsorbent materials, and commercial resins. This outstanding adsorption is related to the hollow dandelion-like porous structure of the HAM which facilitates the interaction of the hydroxyl groups, typically present on the surface of nanostructured metal oxides, with the boron. Indeed, boric acid is known to have a strong affinity with polyols by chelation as reported by Bhagyaraj et al. [19].

### 3.8. Adsorption mechanism study

The adsorption mechanism of boron on HAM was investigated using FTIR technique. The spectra of boric acid, HAM, and HAM after adsorption with 200  $\text{mg}\cdot\text{L}^{-1}$  and 1000  $\text{mg}\cdot\text{L}^{-1}$  boron solutions are shown in Fig. S6. It could be observed that the spectral profile of HAM did not change after adsorption. This is mainly due to the fact that the amount of boron adsorbed onto HAM is too small, lower than the detection limit of the FTIR technique.

The XPS technique was also utilized to determine the adsorption mechanism. The spectra of HAM and HAM after adsorption with a 1000  $\text{mg}\cdot\text{L}^{-1}$  boron solution were analyzed, as shown in Fig. 4. Similar to the FTIR results, no significant new peaks appeared in the full-scan spectrum after adsorption (see Fig. 4a). However, as shown in Fig. 4b, the presence of a B(1s) contribution confirms the successful adsorption of boron

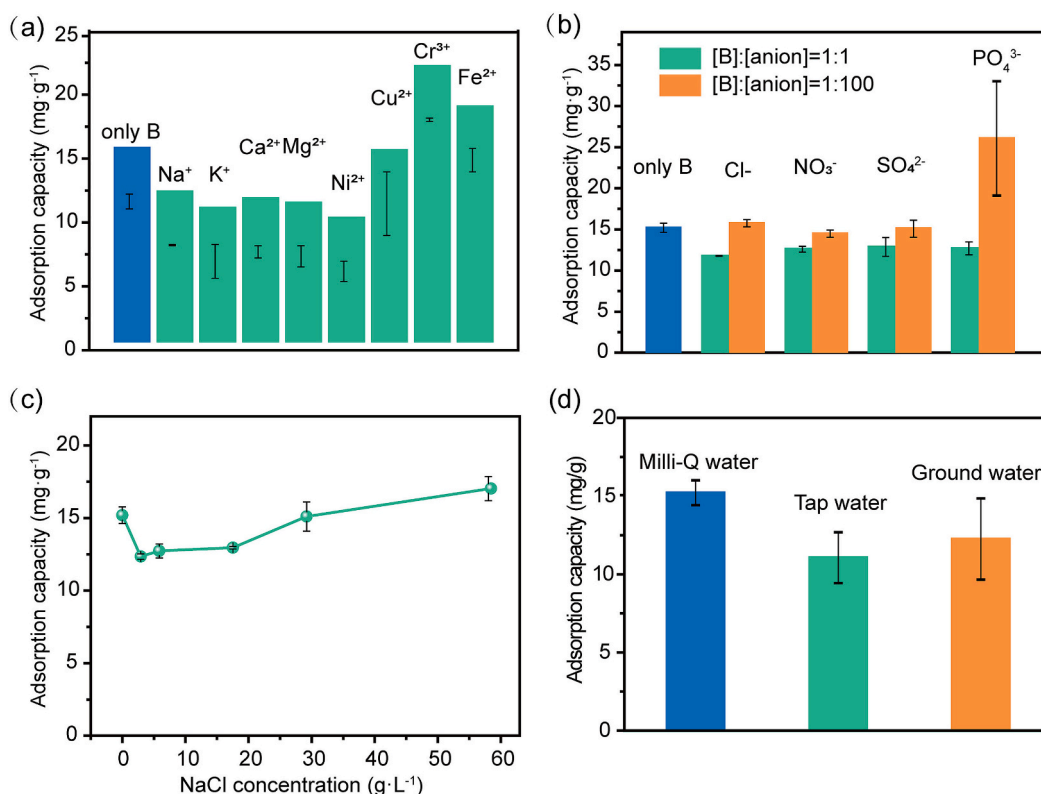


Fig. 3. Adsorption capacity of boron in the presence of competing cations (a), anions (b), different ionic strengths (c), and in simulated real waters (d).

**Table 4**

Boron maximum adsorption capacities of several inorganic and organic adsorbents, and commercial resins.

Adsorbents	Maximum adsorption capacity ( $\text{mg}\cdot\text{g}^{-1}$ )	Particle size ( $\mu\text{m}$ )	Ref
HAM	138.50	1–2	This work
Activated carbon	0.97	–	[46]
Wood sawdust	1.58	–	[46]
Activated alumina	1.97	–	[47]
Composite alginate-alumina	56.33	800–2300	[48]
Pyrocatechol-modified MCM-41	19.45	$1.3\cdot 10^{-3}$	[49]
MgO-Co-ferrite	0.25	$43\cdot 10^{-3}$	[50]
Li/Al-LDHs	42.91	–	[51]
NMDG modified 4-vinylbenzyl chloride	7.19	$28\cdot 10^{-3}$	[52]
NMDG@GPTMS-NBF	17.71	0.3	[53]
CL-RESIN	8.37	722–855	[54]
NCL-RESIN	8.57	710–845	[54]
IRA743-RESIN	10.92	550–700	[54]
P(GMA-co-TRIM)-EN-PG-RESIN	29.22	<241	[55]
P(GMA-co-TRIM)-TETA-PG-RESIN	23.25	<273	[55]
T-RESIN	21.25	–	[56]

on the HAM. Compared with the spectrum of boric acid, the binding energy of B(1s) in HAM appears at lower energy 192.61 eV, instead of 193.4 eV, after adsorption, indicating the formation of a bond. Furthermore, the binding energy at Al(2p) (see Fig. 4c) and O(1s) (see Fig. 4d) decreased after adsorption, which was attributed to the bonding of adsorbent with boron species at higher pH values than the point of zero charge [43]. All these results are consistency with previous studies [44,45] and strongly indicate the formation of Al-O-B bonds.

### 3.9. Adsorption-desorption study

For practical applications, the regeneration capability of adsorbents is a key parameter to assess. The adsorption capacity did not show significant change after the 1st regeneration (see Fig. 5). From the 2nd to 5th regeneration cycle, the adsorption capacity of HAM shows only a slight decrease (<15.28 %) which demonstrates that this material has a good regeneration capabilities regarding boron adsorption.

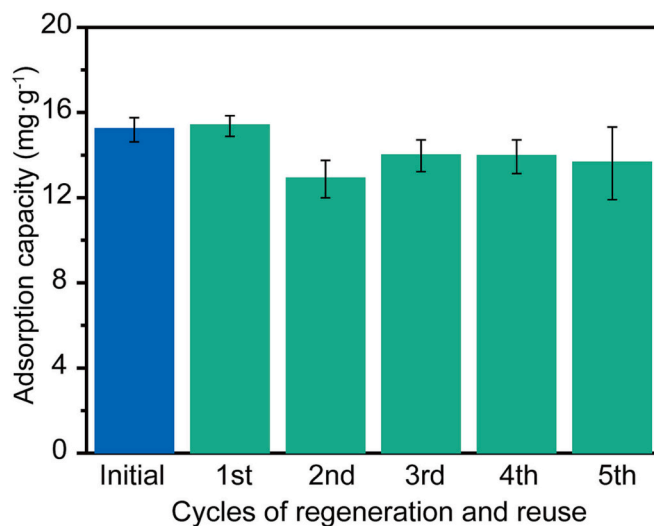


Fig. 5. Adsorption capacity of boron after various adsorption/desorption cycles.

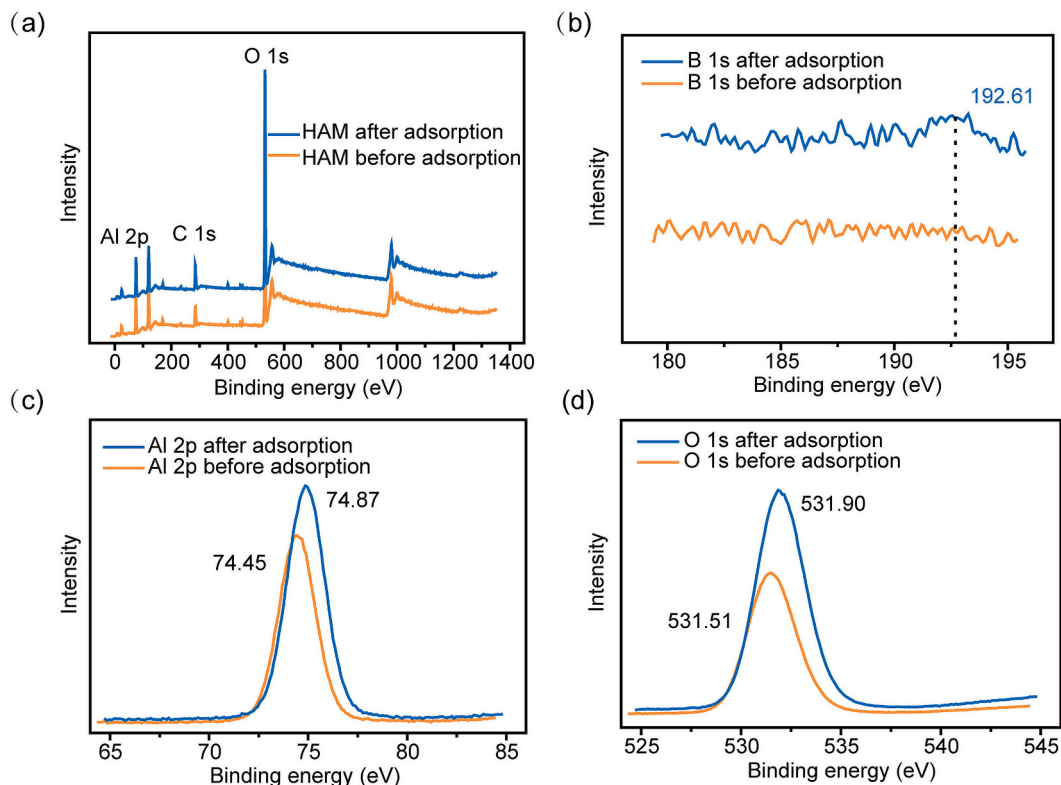


Fig. 4. XPS spectra of HAM before and after adsorption. Full-scan spectrum (a), B 1s (b), Al 2p (c), and O 1s (d).

## 4. Conclusions

In this study, HAM hollow spherical particles ( $\sim 1.5 \mu\text{m}$ ) with a porous dandelion structure were synthesized through a microwave-assisted co-precipitation method and used for effective boron removal from aqueous solutions. The modeling of the adsorption isotherm and the kinetics indicated that single-layer homogeneous adsorption occurs (Langmuir) and that chemical adsorption was the controlling step in the adsorption (pseudo-second order). The obtained adsorption capacity at  $800 \text{ mg}\cdot\text{L}^{-1}$  initial concentration was  $51.60 \text{ mg}\cdot\text{g}^{-1}$  and the theoretical maximum capacity calculated was  $138.50 \text{ mg}\cdot\text{g}^{-1}$ , which is higher than many adsorbents that have been previously reported in the literature.

According to the analysis of the thermodynamic parameters,  $\Delta H^\circ$  is negative and  $\Delta G^\circ$  is positive which indicates that the adsorption of boron on HAM is an exothermic and non-spontaneous process. HAM also showed excellent selectivity towards boron in an aqueous solution in the presence of competitive salt ions ( $\text{Na}^+$ ,  $\text{K}^+$ ,  $\text{Ca}^{2+}$ ,  $\text{Mg}^{2+}$ ), metal ions ( $\text{Cu}^{2+}$ ,  $\text{Cr}^{2+}$ ,  $\text{Ni}^{2+}$ , and  $\text{Fe}^{2+}$ ), anions ( $\text{Cl}^-$ ,  $\text{NO}_3^-$ ,  $\text{SO}_4^{2-}$ ,  $\text{PO}_4^{3-}$ ) and different ion strengths. The XPS spectra of HAM after adsorption indicated the formation of new Al-O-B bonds. In addition, no significant decrease in the adsorption performance was observed after five regeneration cycles. Therefore, HAM can be a promising adsorbent material for boron removal from contaminated water in industrial applications.

## Declaration of competing interest

The authors declare that they have no known competing financial interests or personal relationships that could have appeared to influence the work reported in this paper.

## Data availability

Data will be made available on request.

## Acknowledgments

This research was financially supported by the project CTM2015-65414-C2-1-R from the MINECO ministry of Spain. X.-Y. Lou acknowledges the China scholarship council for the fellowship (201708110179). R. Boada acknowledges funding support from the European Union's Horizon 2020 research and innovation program under the Marie Skłodowska-Curie grant agreement No. 665919. L. Yohai acknowledges Agencia Nacional de Promoción Científica y Tecnológica for PICT funding (grant PICT 2019-00565) and BEC.AR programme (call 2019).

## Appendix A. Supplementary data

Supplementary data to this article can be found online at <https://doi.org/10.1016/j.jwpe.2023.104218>.

## References

- [1] Q. Wang, T. Chen, P. Bai, J. Lyu, X. Guo,  $\text{Fe}_3\text{O}_4$ -loaded ion exchange resin for chromatographic separation of boron isotopes: experiment and numerical simulation, *Chem. Eng. Res. Des.* 171 (2021) 358–366, <https://doi.org/10.1016/j.cherd.2021.05.023>.
- [2] P.F. Rodríguez-Espinoza, C. Sabarathinam, K.M. Ochoa-Guerrero, E. Martínez-Tavera, B. Panda, Geochemical evolution and boron sources of the groundwater affected by urban and volcanic activities of Puebla Valley, south central Mexico, *J. Hydrol.* 584 (2020), 124613, <https://doi.org/10.1016/j.jhydrol.2020.124613>.
- [3] M. Rékási, P. Ragályi, A. Füzy, N. Uzinger, P. Dobosy, G. Záray, N. Szűcs-Vásárhelyi, A. Makó, T. Takács, Effect of the boron concentration in irrigation water on the elemental composition of edible parts of tomato, green bean, potato, and cabbage grown on soils with different textures, *Front. Plant Sci.* 12 (2021), <https://doi.org/10.3389/fpls.2021.658892>.
- [4] D. Escarabajal-Henarejos, D. Parras-Burgos, L. Ávila-Dávila, F.J. Cánovas-Rodríguez, J.M. Molina-Martínez, Study of the influence of temperature on boron concentration estimation in desalinated seawater for agricultural irrigation, *Water* 13 (2021) 322, <https://doi.org/10.3390/w13030322>.
- [5] F.S. Kot, Boron in the Environment, *Boron Separation Processes* 35, 2015, pp. 1–33, <https://doi.org/10.1016/B978-0-444-63454-2.00001-0>.
- [6] J.-Y. Lin, N.N.N. Mahasti, Y.-H. Huang, Recent advances in adsorption and coagulation for boron removal from wastewater: a comprehensive review, *J. Hazard. Mater.* 407 (2021), 124401, <https://doi.org/10.1016/j.jhazmat.2020.124401>.
- [7] J. Kluczk, T. Korolewicz, M. Zolotajkin, J. Adamek, Boron removal from water and wastewater using new polystyrene-based resin grafted with glycidol, *Water Resour. Ind.* 11 (2015) 46–57, <https://doi.org/10.1016/j.wri.2015.05.001>.
- [8] C. Wang, Z. Kong, L. Duan, F. Deng, Y. Chen, S. Quan, X. Liu, Y. Cha, Y. Gong, C. Wang, Y. Shi, W. Gu, Y. Fu, D. Liang, J.P. Giesy, H. Zhang, S. Tang, Reproductive toxicity and metabolic perturbations in male rats exposed to boron, *Sci. Total Environ.* 785 (2021), 147370, <https://doi.org/10.1016/j.scitotenv.2021.147370>.
- [9] N. Najid, S. Kouzbou, A. Ruiz-García, S. Fellaou, B. Gourich, Y. Stiriba, Comparison analysis of different technologies for the removal of boron from seawater: a review, *J. Environ. Chem. Eng.* 9 (2021), 105133, <https://doi.org/10.1016/j.jece.2021.105133>.
- [10] T.M. Ting, M.M. Nasef, D. Aravindan, I.F.N. Rossan, N. Ruslan, Selective removal of boron from industrial wastewater containing high concentration of ammonia by radiation grafted fibrous adsorbent in fixed bed column, *J. Environ. Chem. Eng.* 9 (2021), 104993, <https://doi.org/10.1016/j.jece.2020.104993>.
- [11] N. Kabay, E. Güler, M. Bryjak, Boron in seawater and methods for its separation - a review, *Desalination* 261 (2010) 212–217, <https://doi.org/10.1016/j.desal.2010.05.033>.
- [12] X.-Y. Lou, R. Boada, V. Verdugo, L. Simonelli, G. Pérez, M. Valiente, Decoupling the adsorption mechanisms of arsenate at molecular level on modified cube-shaped sponge loaded superparamagnetic iron oxide nanoparticles, *J. Environ. Sci.* 121 (2022) 1–12, <https://doi.org/10.1016/j.jes.2021.09.001>.
- [13] J. Kluczk, W. Pudło, K. Krukiewicz, Boron adsorption removal by commercial and modified activated carbons, *Chem. Eng. Res. Des.* 147 (2019) 30–42, <https://doi.org/10.1016/j.cherd.2019.04.021>.
- [14] J. Ulatowska, I. Polowczyk, A. Bastrzyk, T. Koźlecki, W. Sawiński, Fly ash as a sorbent for boron removal from aqueous solutions: equilibrium and thermodynamic studies, *Sep. Sci. Technol.* 55 (2020) 2149–2157, <https://doi.org/10.1080/01496395.2019.1612434>.
- [15] S. Bai, S. Chen, J. Li, R. Ya, N. Ao, J. Wang, Effect of silicon on the mathematical model prediction and adsorption mechanism of boron removal by a fixed-bed column, *J. Water Process Eng.* 49 (2022), 103194, <https://doi.org/10.1016/j.jwpe.2022.103194>.
- [16] R. Saavedra, R. Muñoz, M.E. Taboada, M. Vega, S. Bolado, Comparative uptake study of arsenic, boron, copper, manganese and zinc from water by different green microalgae, *Bioresour. Technol.* 263 (2018) 49–57, <https://doi.org/10.1016/j.biortech.2018.04.101>.
- [17] A.A. Oladipo, M. Gazi, Targeted boron removal from highly-saline and boron-spiked seawater using magnetic nanobeads: chemometric optimisation and modelling studies, *Chem. Eng. Res. Des.* 121 (2017) 329–338, <https://doi.org/10.1016/j.cherd.2017.03.024>.
- [18] J. Kluczk, J. Trojanowska, M. Zolotajkin, J. Ciba, M. Turek, P. Dydo, Boron removal from wastewater using adsorbents, *Environ. Technol.* 28 (2007) 105–113, <https://doi.org/10.1080/09593332808618769>.
- [19] S. Bhagayaraj, M.A. Al-Ghouti, P. Kasak, I. Krupa, An updated review on boron removal from water through adsorption processes, *Emerg. Mater.* 4 (2021) 1167–1186, <https://doi.org/10.1007/s42247-021-00197-3>.
- [20] H. Bessaies, S. Iftikhar, B. Doshi, J. Kheriji, M.C. Ncibi, V. Srivastava, M. Sillanpää, B. Hamrouni, Synthesis of novel adsorbent by intercalation of biopolymer in LDH for the removal of arsenic from synthetic and natural water, *J. Environ. Sci.* 91 (2020) 246–261, <https://doi.org/10.1016/j.jes.2020.01.028>.
- [21] K. Li, H. Liu, S. Li, Q. Li, S. Li, Q. Wang, The determinants of effective defluorination by the LiAl-LDHs, *J. Environ. Sci.* 126 (2023) 153–162, <https://doi.org/10.1016/j.jes.2022.04.050>.
- [22] J. Xiao, H. Ji, Z. Shen, W. Yang, C. Guo, S. Wang, X. Zhang, R. Fu, F. Ling, Self-assembly of flower-like  $\gamma\text{-AlOOH}$  and  $\gamma\text{-Al}_2\text{O}_3$  with hierarchical nanoarchitectures and enhanced adsorption performance towards methyl orange, *RSC Adv.* 4 (2014) 35077–35083, <https://doi.org/10.1039/C4RA05343E>.
- [23] W. Cai, J. Yu, M. Jaroniec, Template-free synthesis of hierarchical spindle-like  $\gamma\text{-Al}_2\text{O}_3$  materials and their adsorption affinity towards organic and inorganic pollutants in water, *J. Mater. Chem.* 20 (2010) 4587, <https://doi.org/10.1039/b924366f>.
- [24] T.M. Salman, R.K. Fakher Alfahed, H.A. Badran, K.I. Ajeel, M.M. Jafer, K. K. Mohammad, The evaluation and analysing the boron concentration rate in soil of north Basrah city (Iraq) by carmine method, in: *Journal of Physics: Conference Series*, IOP Publishing, 2019, p. 22006, <https://doi.org/10.1088/1742-6596/1294/2/022006>.
- [25] S.G. Lanas, M. Valiente, E. Aneggi, A. Trovarelli, M. Tolazzi, A. Melchior, Efficient fluoride adsorption by mesoporous hierarchical alumina microspheres, *RSC Adv.* 6 (2016) 42288–42296, <https://doi.org/10.1039/C5RA27371D>.
- [26] J.O. Amode, J.H. Santos, Z.Md. Alam, A.H. Mirza, C.C. Mei, Adsorption of methylene blue from aqueous solution using untreated and treated (Metroxylon spp.) waste adsorbent: equilibrium and kinetics studies, *Int. J. Ind. Chem.* 7 (2016) 333–345, <https://doi.org/10.1007/s40090-016-0085-9>.
- [27] L. Smrčok, V. Langer, J. Křešlák,  $\gamma\text{-Alumina}$ : a single-crystal X-ray diffraction study, *Acta Crystallogr. Sect. C: Cryst. Struct. Commun.* 62 (2006) i83–i84, <https://doi.org/10.1107/S0108270106026850>.
- [28] C.M. Evans, D.L. Sparks, On the chemistry and mineralogy of boron in pure and in mixed systems: a review, *Commun. Soil Sci. Plant Anal.* 14 (1983) 827–846, <https://doi.org/10.1080/00103628309367412>.

- [29] K. Chruszcz-Lipska, B. Winid, G.A. Madalska, J. Macuda, Ł. Łukański, High content of boron in curative water: from the spa to industrial recovery of borates? (Poland as a case study), *Minerals* 11 (2020) 8, <https://doi.org/10.3390/min11010008>.
- [30] L. Cai, Y. Zhang, X. Peng, F. Guo, L. Ji, L. Li, Preparation of layered double hydroxide intercalated by gallic acid for boron adsorption, *J. Water Process Eng.* 44 (2021), 102394, <https://doi.org/10.1016/j.jwpe.2021.102394>.
- [31] S. Bhagyaraj, M.A. Al-Ghouti, M. Khan, P. Kasak, I. Krupa, Modified os sepiae of *Sepiella inermis* as a low cost, sustainable, bio-based adsorbent for the effective remediation of boron from aqueous solution, *Environ. Sci. Pollut. Res.* 29 (2022) 71014–71032, <https://doi.org/10.1007/s11356-022-20578-3>.
- [32] F. Steiner, M. do C. Lana, Effect of pH on boron adsorption in some soils of Paraná, Brazil, Chilean, *J. Agric. Res.* 73 (2013) 28–29, <https://doi.org/10.4067/S0718-58392013000200015>.
- [33] M.A. Al-Ghouti, M. Khan, A. Malik, M. Khraisheh, D. Hijazi, S. Mohamed, S. Alsourour, R. Eltayeb, F. Al Mahmoud, J. Alahmad, Development of novel nano- $\gamma$ - $\text{Al}_2\text{O}_3$  adsorbent from waste aluminum foil for the removal of boron and bromide from aqueous solution, *J. Water Process. Eng.* 50 (2022), 103312, <https://doi.org/10.1016/j.jwpe.2022.103312>.
- [34] X. Hu, L. Jia, J. Cheng, Z. Sun, Magnetic ordered mesoporous carbon materials for adsorption of minocycline from aqueous solution: preparation, characterization and adsorption mechanism, *J. Hazard. Mater.* 362 (2019) 1–8, <https://doi.org/10.1016/j.jhazmat.2018.09.003>.
- [35] S.K. Singh, T.G. Townsend, D. Mazyck, T.H. Boyer, Equilibrium and intra-particle diffusion of stabilized landfill leachate onto micro- and meso-porous activated carbon, *Water Res.* 46 (2012) 491–499, <https://doi.org/10.1016/j.watres.2011.11.007>.
- [36] K. Wang, L. Boithias, Z. Ning, Y. Han, S. Sauvage, J.M. Sánchez-Pérez, K. Kuramochi, R. Hatano, Comparison of Langmuir and Freundlich adsorption equations within the SWAT-K model for assessing potassium environmental losses at basin scale, *Agric. Water Manag.* 180 (2017) 205–211, <https://doi.org/10.1016/j.agwat.2016.08.001>.
- [37] C. Ng, J.N. Lasso, W.E. Marshall, R.M. Rao, Freundlich adsorption isotherms of agricultural by-product-based powdered activated carbons in a geosmin-water system, *Bioresour. Technol.* 85 (2002) 131–135, [https://doi.org/10.1016/S0960-8524\(02\)00093-7](https://doi.org/10.1016/S0960-8524(02)00093-7).
- [38] J.H. Potgieter, Adsorption of methylene blue on activated carbon: an experiment illustrating both the Langmuir and Freundlich isotherms, *J. Chem. Educ.* 68 (1991) 349–350, <https://doi.org/10.1021/ed068p349>.
- [39] J. Kluczk, A. Tórz, D. Łacka, A. Kazek-Kęsik, J. Adamek, Boron removal by adsorption on cobalt(II) doped chitosan bio-composite, *J. Polym. Environ.* 26 (2018) 2039–2048, <https://doi.org/10.1007/s10924-017-1099-x>.
- [40] A.A. Oladipo, M. Gazi, Hydroxyl-enhanced magnetic chitosan microbeads for boron adsorption: parameter optimization and selectivity in saline water, *React. Funct. Polym.* 109 (2016) 23–32, <https://doi.org/10.1016/j.reactfunctpolym.2016.09.005>.
- [41] Y.-T. Wei, Y.-M. Zheng, J.P. Chen, Design and fabrication of an innovative and environmental friendly adsorbent for boron removal, *Water Res.* 45 (2011) 2297–2305, <https://doi.org/10.1016/j.watres.2011.01.003>.
- [42] C.O. Anuo, S. Rakshit, M.E. Essington, Influence of oxytetracycline on boron adsorption at the hematite–water interface: a macroscopic and in situ ATR–FTIR study, *Soil Sci. Soc. Am. J.* 85 (2021) 606–618, <https://doi.org/10.1002/saj2.20235>.
- [43] T. Chen, J. Lyu, Q. Wang, P. Bai, Y. Wu, X. Guo, Mechanistic study on boron adsorption and isotopic separation with magnetic magnetite nanoparticles, *J. Mater. Sci.* 56 (2021) 4624–4640, <https://doi.org/10.1007/s10853-020-05546-x>.
- [44] T. Chen, Q. Wang, J. Lyu, P. Bai, X. Guo, Boron removal and reclamation by magnetic magnetite ( $\text{Fe}_3\text{O}_4$ ) nanoparticle: an adsorption and isotopic separation study, *Sep. Purif. Technol.* 231 (2020), 115930, <https://doi.org/10.1016/j.seppur.2019.115930>.
- [45] F. Meng, W. Ma, L. Wu, H. Hao, L. Xin, Z. Chen, M. Wang, Selective and efficient adsorption of boron (III) from water by 3D porous CQDs/LDHs with oxygen-rich functional groups, *J. Taiwan Inst. Chem. Eng.* 83 (2018) 192–203, <https://doi.org/10.1016/j.jtice.2017.12.008>.
- [46] M. Jaouadi, Characterization of activated carbon, wood sawdust and their application for boron adsorption from water, *Int. Wood Prod. J.* 12 (2021) 22–33, <https://doi.org/10.1080/20426445.2020.1785605>.
- [47] J. Kluczk, J. Ciba, J. Trojanowska, M. Zolotajkin, M. Turek, P. Dydo, Removal of boron dissolved in water, *Environ. Prog.* 26 (2007) 71–77, <https://doi.org/10.1002/ep.10180>.
- [48] Barron-Zambrano Demey, Miloudi Mhadhbi, Ruiz Yang, Sastre, Boron removal from aqueous solutions by using a novel alginate-based sorbent: comparison with  $\text{Al}_2\text{O}_3$  particles, *Polymers* 11 (2019) 1509, <https://doi.org/10.3390/polym11091509>.
- [49] Y. Chen, J. Lyu, Y. Wang, T. Chen, Y. Tian, P. Bai, X. Guo, Synthesis, characterization, adsorption, and isotopic separation studies of pyrocatechol-modified MCM-41 for efficient boron removal, *Ind. Eng. Chem. Res.* 58 (2019) 3282–3292, <https://doi.org/10.1021/acs.iecr.8b04748>.
- [50] C.N. Pinotti, L.M. de Souza, W.P. Marques, J.R.C. Proveti, H.C. Jesus, J.C.C. Freitas, P.S.S. Porto, E.P. Muniz, E.C. Passamani, A new magnetic composite with potential application in boron adsorption: development, characterization, and removal tests, *Mater. Chem. Phys.* 277 (2022), 125368, <https://doi.org/10.1016/j.matchemphys.2021.125368>.
- [51] Y. Pan, J. Du, J. Chen, C. Lian, S. Lin, J. Yu, Interlayer intercalation of Li/Al-LDHs responsible for high-efficiency boron extraction, *Desalination* 539 (2022), 115966, <https://doi.org/10.1016/j.desal.2022.115966>.
- [52] A. Abbasi, W.Z.N. Yahya, M.M. Nasef, M. Moniruzzaman, A.S.M. Ghumman, H. K. Afolabi, Boron removal by glucamine-functionalized inverse vulcanized sulfur polymer, *React. Funct. Polym.* 177 (2022), 105311, <https://doi.org/10.1016/j.reactfunctpolym.2022.105311>.
- [53] Y. Zhang, X. Liang, T. Jiang, Z. Chen, X. Ji, Removal of boron from aqueous solutions by N-methyl-D-glucamine- $\gamma$ -glycidoxypyrrol-trimethoxysilane with nonwoven basalt fibers support, *Mater. Today Commun.* 31 (2022), 103611, <https://doi.org/10.1016/j.mtcomm.2022.103611>.
- [54] J. Lyu, Z. Zeng, N. Zhang, H. Liu, P. Bai, X. Guo, Pyrocatechol-modified resins for boron recovery from water: synthesis, adsorption and isotopic separation studies, *React. Funct. Polym.* 112 (2017) 1–8, <https://doi.org/10.1016/j.reactfunctpolym.2016.12.016>.
- [55] Q. Luo, M. Zeng, X. Wang, H. Huang, X. Wang, N. Liu, X. Huang, Glycidol-functionalized macroporous polymer for boron removal from aqueous solution, *React. Funct. Polym.* 150 (2020), 104543, <https://doi.org/10.1016/j.reactfunctpolym.2020.104543>.
- [56] S. Bai, J. Han, C. Du, J. Li, W. Ding, Removal of boron and silicon by a modified resin and their competitive adsorption mechanisms, *Environ. Sci. Pollut. Res.* 27 (2020) 30275–30284, <https://doi.org/10.1007/s11356-020-09308-9>.